NSRRC-J04454(2014)

Macromolecules

Article

pubs.acs.org/Macromolecules

Intrinsic Metastability of the α′ Phase and Its Partial Transformation into α Crystals during Isothermal Cold-Crystallization of Poly(L-lactide)

Chia-Ying Chen,[†] Ching-Feng Yang,[†] U-Ser Jeng,[†,‡] and An-Chung Su*[,†]

[†]Department of Chemical Engineering, National Tsing Hua University, Hsinchu 30013, Taiwan

[‡]National Synchrotron Radiation Research Center, Science-Based Industrial Park, Hsinchu 30076, Taiwan

ABSTRACT: Structural evolution of poly(L-lactide) during cold-crystallization at 80 °C was examined via simultaneous small/wide-angle X-ray scattering (SAXS/WAXS), Fourier-transform infrared spectroscopy (FTIR), and differential scanning calorimetry (DSC). The incipient α′ crystals of loosely packed 10_7 helices, formed at t_c = 200 s as detected via both WAXS and FTIR, were hardly identifiable via SAXS or DSC due to its low values of density contrast or latent heat (initially $\Delta H_{\alpha'} \approx 12$ J/g, gradually reaching 74 J/g near the end of crystallization, in contrast to $\Delta H_{\alpha} \approx 140$ J/g), was already large in lateral size (with coherence length $\Lambda_{200/110} \approx 35$ nm, increasing to 50 nm during t_c = 200–400 s and remained little changed afterward). Once formed, the α′ crystals underwent continuous and persistent perfection for decreasing lattice spacing and partially transformed to smaller α crystals ($t_c \approx$ 800–1800 s, up to a saturated population ratio of 1:4 between α and α′ phases), followed by slower yet steady increases in SAXS invariant without significant changes in the α and α′ contents for t_c > 1800 s. It is concluded that the α′ form is a transient structure of continuously increasing packing density and latent heat toward the α form, reminiscent of the mesomorphic phase as precursors to stable crystals in other polymers. Nevertheless, transformation to α crystals occurred when the lattice parameters of the α′ phase were closer but still finitely different from those of the α phase and that the conversion between the two phases was limited in this isothermal case. Both observations suggest that, in spite of the transient nature of the α′ phase, the final transformation step to the stable α form is still achieved via a first-order route.

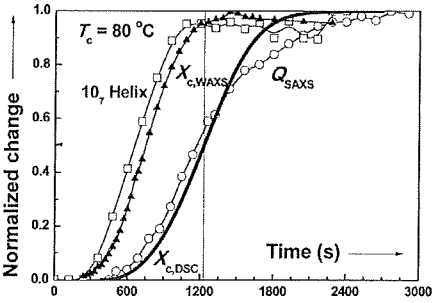

INTRODUCTION

Melt-crystallization of poly(L-lactide) (PLLA) is generally known to give α crystals consisting of two left-handed 10_7 helices in an orthorhombic unit cell with lattice parameters a = 10.8 Å, b = 6.2 Å, and c = 28.8 Å (space group $P2_12_12_1$) as the thermodynamically favored form.[1] However, there emerges a kinetically competitive α′ form at crystallization temperatures (T_c) below 120 °C.[2] The α′ form comprises the same 10_7 helices yet with delicate differences in lateral packing. Compared to the α form with intense $(200)_\alpha/(110)_\alpha$ reflection at scattering vector q = 1.18 Å^{-1} ($d_{200/110}$ = 5.31 Å), and (203) reflection at q = 1.35 Å^{-1} (d_{203} = 4.65 Å) in room-temperature wide-angle X-ray scattering (WAXS) profiles, the corresponding reflections of the α′ form are shifted to q = 1.16 Å^{-1} ($d_{200/110}$ = 5.41 Å) and 1.32 Å^{-1} (d_{203} = 4.75 Å) while the weaker (210) and (103)/(004) reflections become extinct.[1,2] These observations indicate expanded unit cell dimension (by ca. 2.4% in volume) and higher symmetry (i.e., presence of conformational disorder and interchain slippage) for the α′ phase.[1]

It is then interesting to note the peculiar discontinuity of crystallization kinetics of PLLA around 110 °C.[3−5] The maximum of spherulitic growth rate is located at ca. 130 °C, but there is a second maximum around 105 °C, attributed to the competition between α vs α′ forms of different growth characteristics, with the α form dominating at T_c > 110 °C and the α′ form at T_c < 110 °C. Without differentiation in phase composition, the lumped crystal thickness (l_c), long period (L), and coherence length (or crystallite size, Λ) all exhibit their minimum values at ca. 120 °C.[3−6] Specifically, small-angle X-ray scattering (SAXS) results of Kawai et al.[7] indicated decreasing L with increasing T_c from 90 to 120 °C, which was explained by considering mixed α′ and α crystals with T_c-dependent volume fractions. Upon heating of PLLA specimens fully crystallized at T_c < 120 °C, Kawai et al.[7] observed that $d_{200/110}$ decreased quickly around 150 °C and more gradually afterward before fully reaching the α form, indicating occurrence of α′-to-α transformation after 150 °C. As there were no discernible changes in total WAXS and SAXS intensities during the phase transition process, Kawai et al.[7] proposed that the transformation corresponded to a direct *solid–solid* transition process, explicitly considering α and α′ forms as two distinct phases. However, an alternative interpretation of Cho and Strobl[6] that α′ crystals are simply an imperfect form of α crystals at low T_c is also consistent with experimental evidence: disorder in the α′ crystals may lead to

Received: June 5, 2014
Revised: July 15, 2014
Published: July 25, 2014

 © 2014 American Chemical Society dx.doi.org/10.1021/ma501167e | *Macromolecules* 2014, 47, 5144–5151

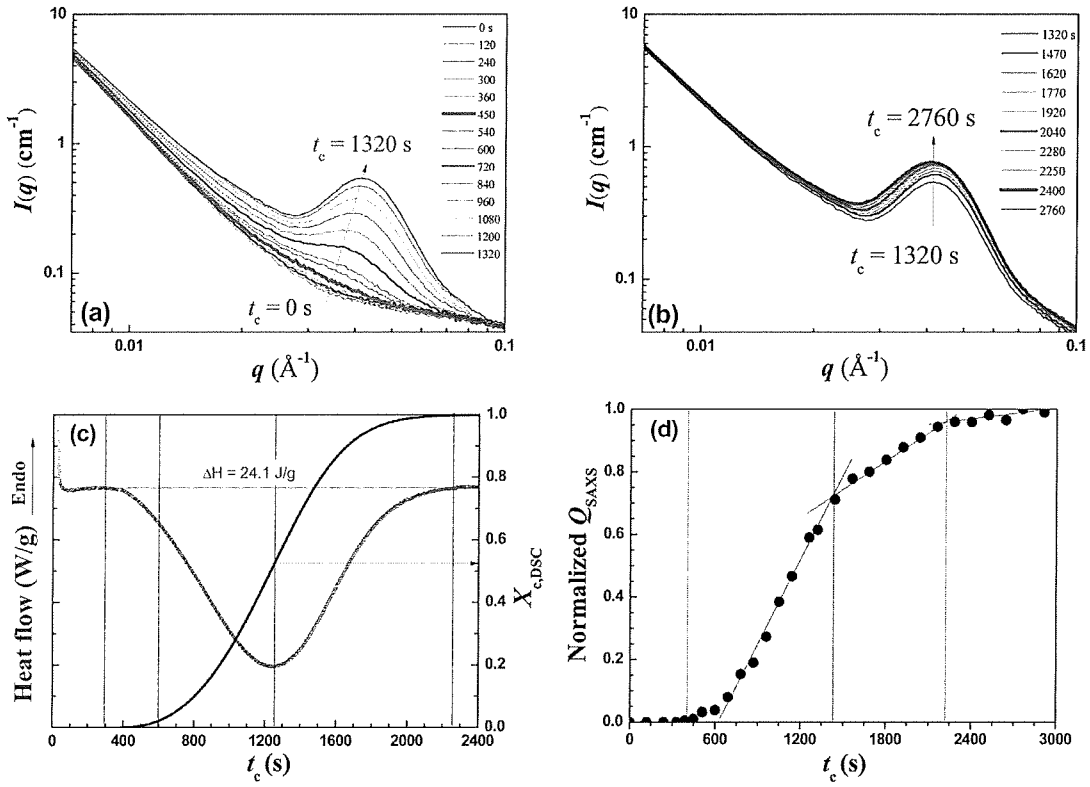

Figure 1. Time-resolved SAXS profiles during cold-crystallization of PLLA at 80 °C for (a) t_c = 0 to 1320 s and (b) t_c = 1320 to 2760 s. Note that the scattering intensity starts to increase after $t_c \approx 360$ s and the scattering peak position (representing average center-to-center intergrain spacing) gradually shifts to higher q values until $t_c \approx 1320$ s and remains constant afterward. (c) Parallel DSC trace showing heat release starting at $t_c \approx 300$ s and ending at $t_c \approx 2260$ s. (d) Sigmoidal rise of Q_{SAXS} starting at $t_c \approx 400$ s, more strongly after $t_c \approx 600$ s, followed by a slower rate beyond $t_c \approx 1400$ s, and finally reaching the plateau value around $t_c \approx 2700$ s.

increased Gibbs free energy and decreased supercooling, hence increased layer thickness; the quantitative transformation from α' to α crystals, as observed by Kawai et al.,[7] simply signifies the kinetic feasibility above 150 °C.

On the basis of simultaneous SAXS/WAXS observations during cold-crystallization of PLLA at 80 °C and with supporting evidence from Fourier-transform infrared spectroscopy (FTIR) and differential scanning calorimetry (DSC) measurements, here we show that the α' form is indeed a transient structure of continuously increasing packing density and latent heat toward the α form, in partial support of the Cho–Strobl interpretation[6] while reminiscent of the mesophase as precursors to stable crystals in some other polymers.[8−20] On the other hand, the fact that transformation to α crystals indeed occurred when the lattice parameters of the α' phase were still finitely different from those of the α phase while the conversion between the two phases remained autoinhibitive (saturated at a population ratio of 1:4 between α and α' phases) in this case of significant density mismatch, consistent with the solid–solid transformation mechanism proposed by Kawai et al.[7] In other words, the transformation from the metastable α' form to the stable α form still involves discontinuities in lattice parameters and a change in crystal symmetry, hence should still be categorized as a first-order transition.

EXPERIMENTAL DETAILS

The PLLA sample ($T_g \approx 55$ °C) with weight-average molecular mass $M_w \approx 120$ kDa and chiral purity of 95%[21] was purchased from Sigma-Aldrich. Prior to use, the sample was purified via precipitation into methanol from chloroform solution, followed by vacuum-drying at 50 °C for a day. Purified specimens sealed in punctured aluminum pans (1 mm in thickness, 6.6 mm in diameter disc) with two Kapton windows (for X-ray incidence) were heated to 210 °C for 3 min to eliminate previous thermal history, followed by quenching into liquid nitrogen to obtain glassy specimens. In-situ SAXS/WAXS measurements were carried out at beamline 23A of the National Synchrotron Radiation Research Center. The melt-quenched glassy PLLA specimens were quickly (100 °C/min) heated in the INSTEC HCS302 sample holder from room temperature to 80 °C for isothermal crystallization up to 40 min. With a 10.5 keV beam (wavelength λ = 1.180 Å), SAXS and WAXS data were collected by use of a Pilatus 1M-F area detector (169 × 179 mm^2) and a Mythen-3K linear detector, respectively. This setup covered the main WAXS reflections of PLLA α' crystals in the q-range of 0.65 to 1.91 Å^{-1} and a SAXS q-range of 0.007 to 0.35 Å^{-1}. The scattering vector $q \equiv 4\pi\lambda^{-1} \sin\theta_B$ (with $2\theta_B$ the scattering angle) was routinely calibrated using polyethylene, tripalmitate, poly(ε-caprolactone) for WAXS and silver behenate for SAXS. All data were further corrected for sample transmission, background, and detector sensitivity.

FTIR spectra were recorded by use of a PerkinElmer Spectrum RXI spectrophotometer equipped with an INSTEC HCS402 high-temperature cell. Spectra were taken at a resolution of 2 cm^{-1} and averaged over 16 scans. Films were cast from chloroform solutions containing 1 wt % PLLA onto KBr pellets ca. 0.4 mm in thickness. Specimens were heated to 210 °C for 3 min, quenched into liquid nitrogen to glassy

dx.doi.org/10.1021/ma501167e | Macromolecules 2014, 47, 5144−5151

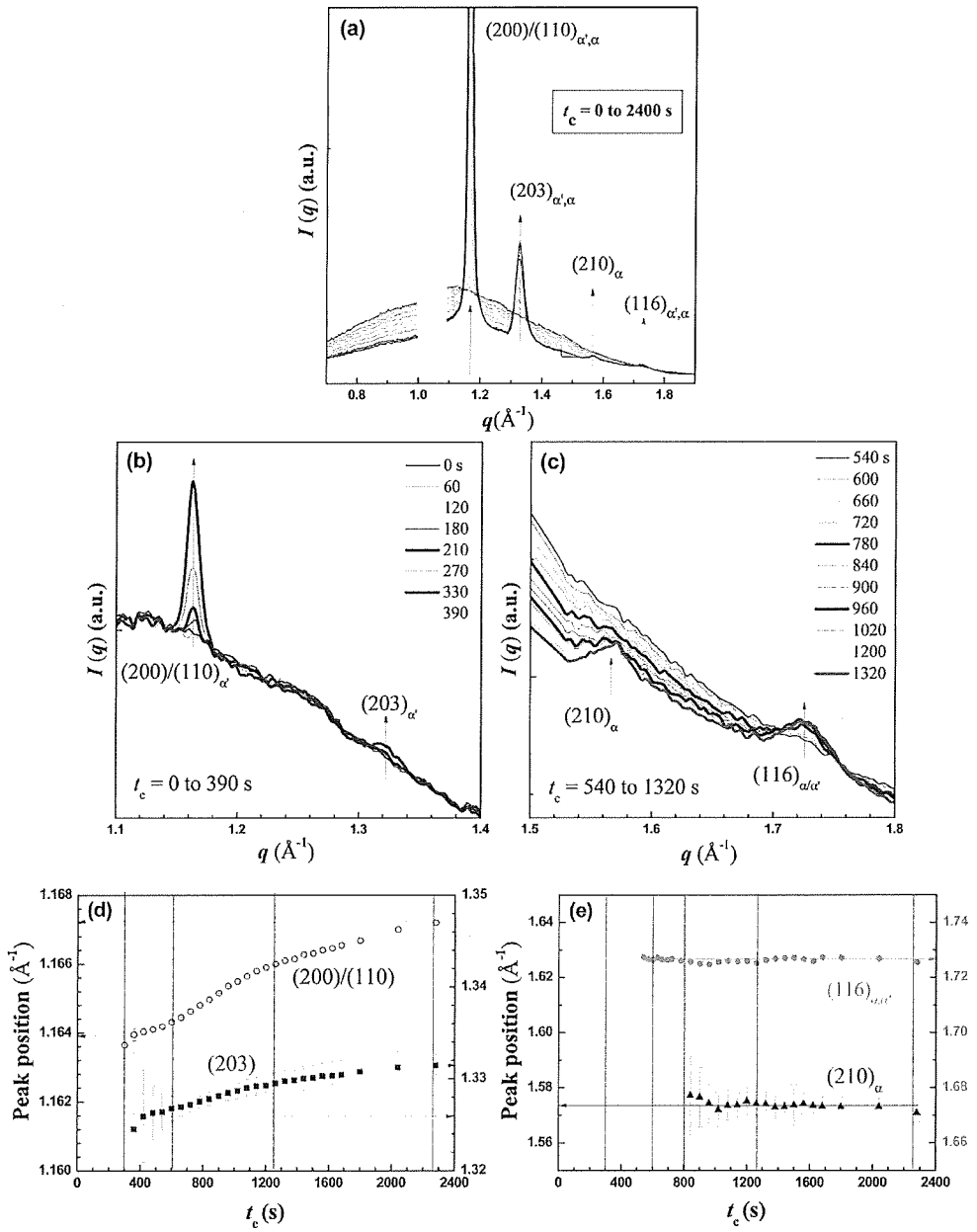

Figure 2. (a) Time-resolved WAXS profiles of PLLA during cold-crystallization at 80 °C. Expanded views are shown in part b for $(200)/(110)_{\alpha'}$ and $(203)_{\alpha'}$ reflections form t_c = 0 to 390 s and part c for $(210)_{\alpha}$ and $(116)_{\alpha,\alpha'}$ reflections form t_c = 540 to 1320 s. It can be observed from part b that α' crystals emerge at $t_c \approx 210$ s, significantly earlier than the start of increase in SAXS intensity at $t_c \approx 330$ s (cf. Figure 1a). Note in particular the emergence of the $(210)_{\alpha}$ reflection around $t_c \approx 900$ s, signifying formation of α crystals even at this relatively low T_c. Clear shifts of (200)/(110) and (203) peak positions with t_c are shown in part d whereas (210) and (116) peak positions remain relatively unchanged in part e. No shifts in peak position can be identified due (at least partly) to increased experimental uncertainty in this case of relatively low WAXS intensity.

state, followed by vacuum-drying for 1/2 h at room temperature for removal of residual solvent. Specimens were then quickly (100 °C/min) heated from room temperature to 80 °C for isothermal crystallization, during which FTIR spectra were continuously taken. The same temperature program was adopted in DSC measurements made (for samples ca. 5 mg in weight) by use of a PerkinElmer Pyris Diamond instrument routinely calibrated with high-purity indium and zinc standards and operated under a steady stream of protective nitrogen. Temperature calibration of INSTEC HCS302 and HCS402 was made by use of 1,3,5-trichlorobenzene, 3,5-dinitrobenzoic acid, benzoic acid, and potassium nitrate, giving extrapolated confidence in temperature accuracy better than ±0.4 °C at 80 °C.

RESULTS

SAXS/DSC Observations. Illustrated in Figure 1a,b are the time-resolved SAXS profiles during cold-crystallization of PLLA specimens upon temperature-jump to 80 °C from the glassy state. Scattering intensity in the low-q range decreases monotonically with increasing q, exhibiting fractal-like depend-

dx.doi.org/10.1021/ma501167e | Macromolecules 2014, 47, 5144−5151

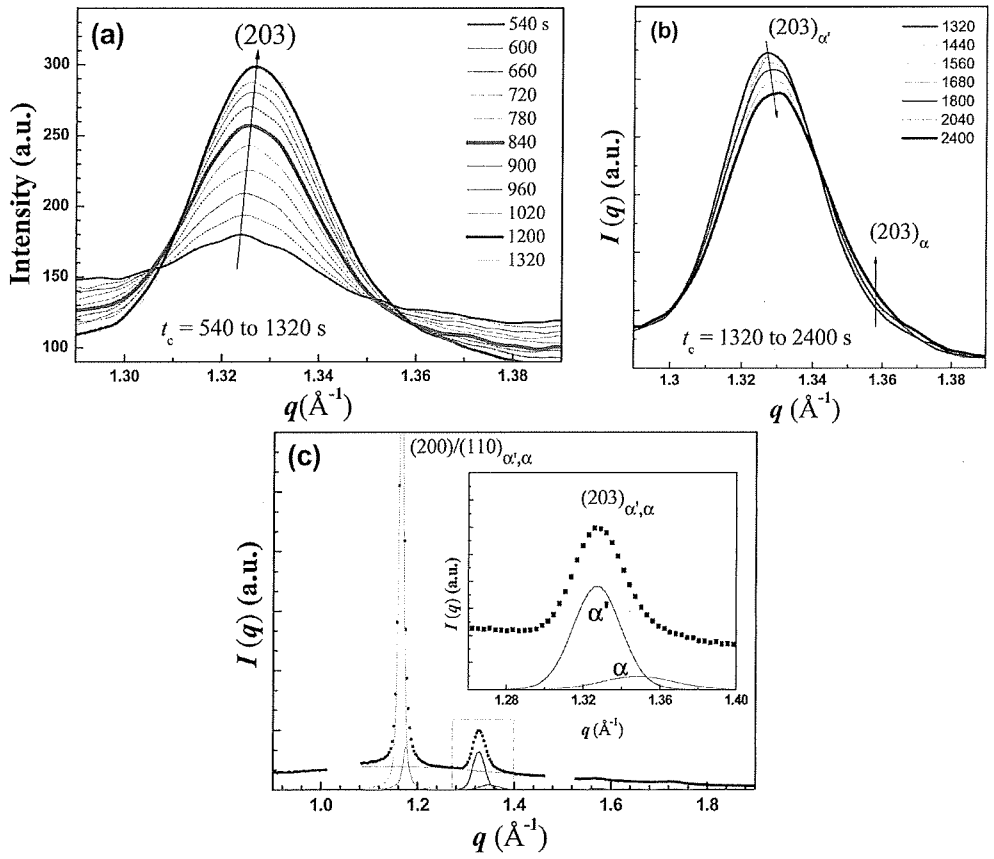

Figure 3. Expanded view of changing (203) peak positions during (a) t_c = 540–1320 s and (b) t_c = 1320–2400 s. High-q shifts of (200)/(110) and (203) reflections are clearly beyond experimental errors. Demonstrated in (c) is the resolution of a representative WAXS profile (obtained at t_c = 1260 s) into contributions from a broad amorphous halo, 6 specific peaks representing $(200)/(110)_{\alpha'}$, $(203)_{\alpha'}$, $(200)/(110)_{\alpha}$, $(203)_{\alpha}$ and $(210)_{\alpha}$ reflections plus a lumped $(116)_{\alpha',\alpha}$ peak due to its low intensity and its relative insensitivity to the α' content at this temperature (cf. Figure 2c).

ence often observed in polymer melts or glasses.[15,18−20,22] The SAXS profiles remain little changed up to $t_c \approx 300$ s, beyond which the SAXS intensity around $q \approx 0.03$ Å^{-1} starts to increase, developing into a broad peak after $t_c \approx 600$ s with gradual high-q shift of its maximum to $q \approx 0.04$ Å^{-1} at $t_c \approx$ 1320 s. This is followed by steady intensity increases in the more limited q-range of 0.03 to 0.07 Å^{-1} without further shifts in peak position (suggesting stabilized nanograin population) or apparent saturation of intensity up to $t_c \approx 2700$ s while the release of latent heat has already completed at $t_c \approx 2260$ s, as indicated by the parallel DSC trace in Figure 1c. This slow but extended increase in peak intensity is more clearly demonstrated by the SAXS invariant $Q_{SAXS} \equiv \int q^2 I(q)\, dq$ (with the integration range operationally chosen as q = 0.007 to 0.1 Å^{-1}) shown in Figure 1d. The increase of Q_{SAXS} starts at $t_c \approx 400$ s, remains slow up to $t_c \approx 600$ s, becomes rapid afterward until $t_c \approx 1400$ s, and then maintains a lowered rate up to $t_c \approx 2700$ s where the plateau value is reached. The gradual high-q shift of peak maximum up to $t_c \approx 1320$ s suggests increasing population of nanograins (i.e., decreasing intergrain spacing)[17−19] whereas the stabilized peak position implies saturated nanograin population. The continuing increase of SAXS invariant Q_{SAXS} ($\equiv \int q^2 I(q)\, dq$ in the operationally chosen integration range of q = 0.007 to 0.1 Å^{-1}) from $t_c \approx 1320$ to 2700 s could imply increasing nanograin size (and hence volume fraction f of the crystalline phase), but this is inconsistent with the completion of thermal event before $t_c \approx 2260$ s. It is more likely that this continuing increase in Q_{SAXS} is mainly due to the increasing density contrast between crystalline nanograins and the amorphous matrix, as supported by the WAXS results below.

WAXS Analysis. Given in Figure 2a are WAXS profiles obtained concomitant with the SAXS measurements. It may be observed first that the initially emerged crystals (at $t_c \approx 200$ s, some 100 s ahead of DSC- or SAXS-identified incipience of crystallization) are in the α' from (Figure 2b,c) consistent with the generally accepted demarcation at $T_c \approx 120$ °C, below which kinetic preference goes to the α' phase. However, formation of α crystals may indeed be identified after $t_c \approx 800$ s (Figure 2c) as indicated by the emergence of characteristic $(210)_{\alpha}$ reflection. Within experimental confidence, there is a general tendency of the α'-related reflections to shift to higher-q positions (Figure 2d) while the later-rising, weak $(210)_{\alpha}$ and $(116)_{\alpha,\alpha'}$ reflections remain comparatively constant (Figure 2e) in their peak positions. The shift in $(110/200)_{\alpha,\alpha'}$ and $(203)_{\alpha,\alpha'}$ peak positions is consistently observed from the incipient emergence of the reflections before and after the emergence of identifiable $(210)_{\alpha}$ intensity, as more clearly demonstrated in Figure 3a,b, indicating continuously increased density of α' crystals via decreased lattice spacing. Note also that, as the $(203)_{\alpha'}$ and $(203)_{\alpha}$ peaks are adequately apart in their positions (ca. 1.33 vs 1.36 Å^{-1}), the latter contribution can be separately identified in Figure 3b. Demonstrated in Figure 3c is the

dx.doi.org/10.1021/ma501167e | Macromolecules 2014, 47, 5144−5151

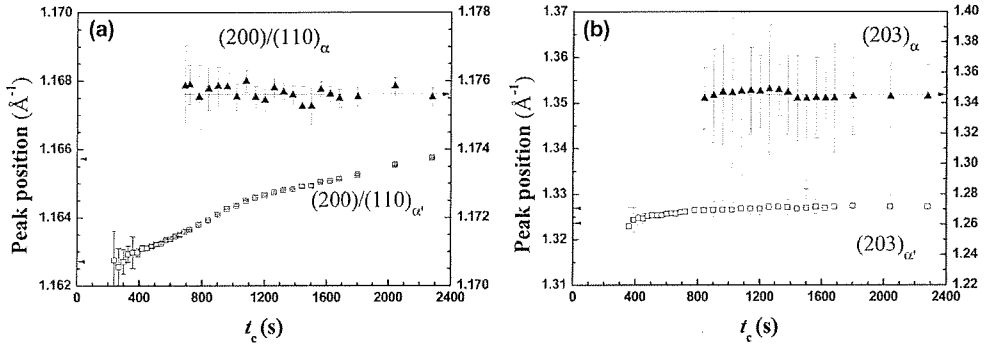

Figure 4. Comparison of (a) (200)/(110) and (b) (203) peak positions of α' and α phases. Note that peak positions of the α' phase shifted to higher q values with increasing t_c whereas those of the α phase remained unaltered. The total changes (up to t_c = 2040 s) in d-spacing values of $(200)/(110)_{\alpha'}$ and $(203)_{\alpha'}$ reflections correspond to ca. 0.26% and 0.22%, respectively, consistent with ca. 0.3% shrinkages in both the a- and b-axes while the c-axis remains unchanged.

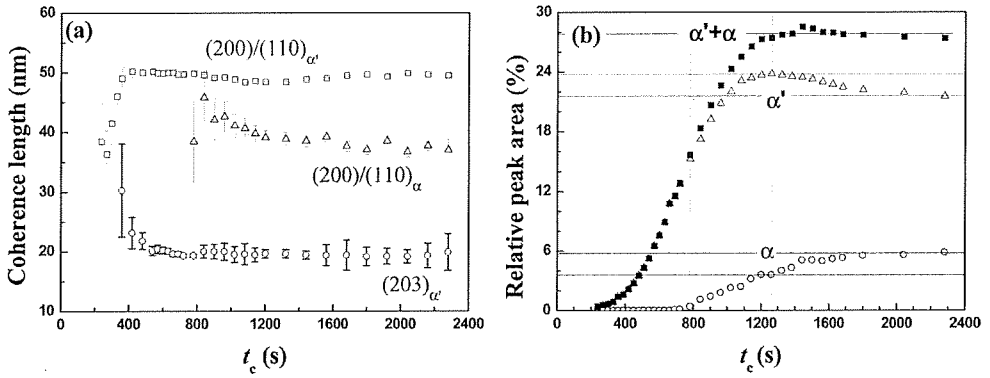

Figure 5. (a) Coherence length calculated from the WAXS peak width using Scherrer's equation. (b) Fractions of WAXS peak areas $f_{\alpha'}$ and f_{α} contributed by α' and α phases, respectively. Note in particular that, after reaching its maximum ($f_{\alpha'}$ = 0.238) at t_c = 1260 s, the population of α' phase decreased to $f_{\alpha'}$ = 0.219 whereas that of the α phase continued to increase from f_{α} = 0.036 to f_{α} = 0.056.

deconvolution of the $(203)_{\alpha,\alpha'}$ peak into contributions from α and α' crystals, resulting consistently in a $(203)_{\alpha}$ reflection of constant peak position and a $(203)_{\alpha'}$ contribution with the peak position continuously shifting toward the higher-q range. Similar observations have also been made on other peaks, as shown in Figure 4, demonstrating the continuous densification of α' crystals once formed. Note that the weak $(116)_{\alpha,\alpha'}$ reflection was not resolved due to its low intensity and its relative insensitivity to the α' content at this temperature (cf. Figure 2c).

From these resolved peaks, coherence length Λ and relative phase fraction f may respectively be calculated from the Scherrer equation and the relative areas contributed from different phases, as summarized in Figure 5. The incipient α' crystals formed at $t_c \approx 200$ s are already large in lateral size, with $\Lambda_{(200)/(110)\alpha'} \approx 37$ nm, followed by quick growth to $\Lambda_{(200)/(110)\alpha'} \approx 49$ nm at $t_c \approx 400$ s and remain nearly unchanged thereafter. The $(203)_{\alpha'}$ reflection emerges at near $t_c \approx 400$ s, with $\Lambda_{(203)\alpha'} \approx 27$ nm, which decreases to ca. 20 nm at $t_c \approx 800$ s and remain little changed afterward. The significantly lower values of $\Lambda_{(203)\alpha'}$ as compared to those of $\Lambda_{(200)/(110)\alpha'}$ indicate that the lateral crystal size is generally large but more limited along the crystal thickness direction. For α crystals incipiently formed at $t_c \approx 800$ s, $\Lambda_{(200)/(110)\alpha} \approx 43$ nm, which gradually decrease to 39 nm near $t_c \approx 1200$ s and eventually to ca. 37 nm near $t_c \approx 2400$ s. The decreasing tendency of average domain size indicates continuously generated smaller crystals of the α form.

Given in Figure 5b are changes in α' and α phase fractions represented by resolved WAXS peak areas. The α' phase emerges around $t_c \approx 200$ s, increases in a sigmoidal manner to a maximum level of $f_{\alpha'} \approx 0.24$ at $t_c \approx 1260$ s and then *decreases* gradually to $f_{\alpha'} \approx 0.22$ at $t_c \approx 2340$ s. The α phase emerges around $t_c \approx 800$ s and then increases monotonically to its final level of $f_{\alpha} \approx 0.06$ at $t_c \approx 2340$ s. The total crystalline fraction $f_c \equiv f_{\alpha'} + f_{\alpha}$ rises in a sigmoidal manner in the t_c range of 300–1260 s to its plateau value of $f_c = 0.28$. The decrease of $f_{\alpha'}$ can be explained only by transformation of existing α' crystals into the α form, as supported by the excellent match of the decrease of $f_{\alpha'}$ and the increase of f_{α} beyond $t_c \approx 1260$ s. In addition, the f_c curve is fairly smooth, without a clear break around $t_c \approx 800$ s. It is thus likely that α crystals in this study are mainly transformed from existing α' crystals as a sequential event; significant contributions from a parallel nucleation-and-growth route for formation of α crystals in competition with the α' crystallization process, if it exists, are limited to $t_c < 1260$ s.

FTIR Observations. Given in Figure 6a are the time-resolved FTIR spectra in the range of 800–1500 cm^{-1}. Starting from $t_c \approx 100$ s (i.e., respectively 100 and 200 s ahead of WAXS- and DSC/SAXS-detected incipience of crystal formation), the absorbance of the (C–H bending-coupled) C–O–C stretching band at 1267 cm^{-1} (characteristic of amorphous phase)

dx.doi.org/10.1021/ma501167e | *Macromolecules* 2014, 47, 5144–5151

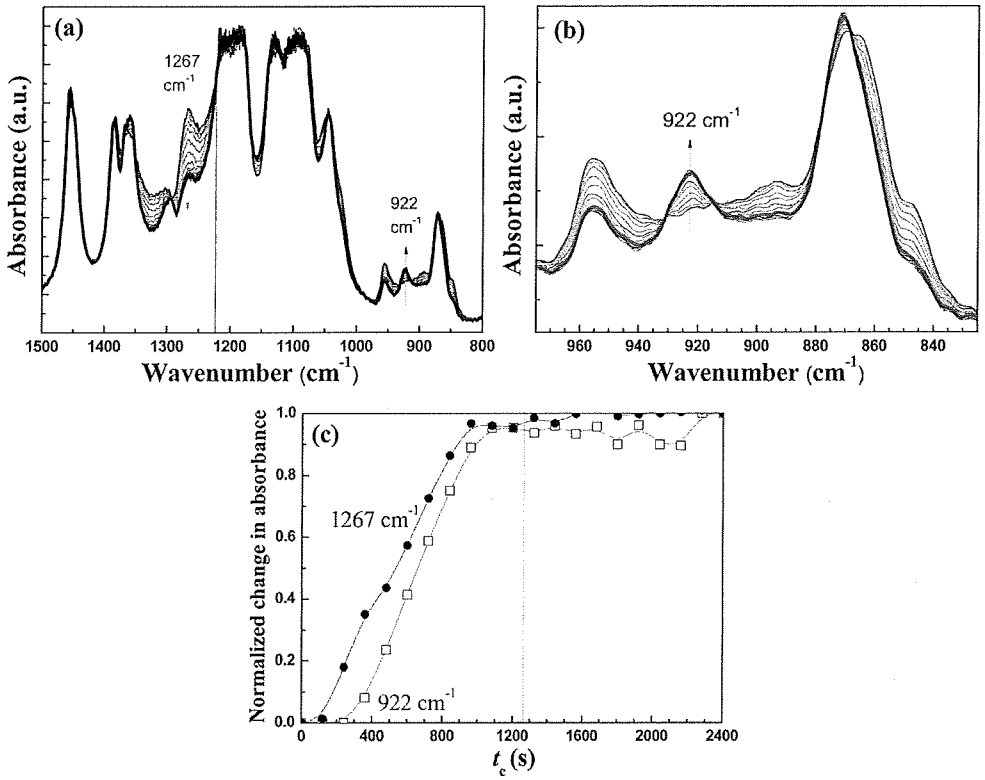

Figure 6. (a) Time-resolved FTIR spectra collected in the spectral range of 800–1500 cm^{-1} during cold-crystallization of PLLA at 80 °C. (b) Expanded view in the 825–975 cm^{-1} range. (c) Normalized changes in absorbance for the helical (integrated between the isosbectic points at 915 to 930 cm^{-1}) and amorphous (integrated from ca. 1250 to 1290 cm^{-1}) bands. There were no significant changes in helical and amorphous bands for $t_c \geq 1260$ s, indicating formation of α crystals from the pre-existing α' crystals.

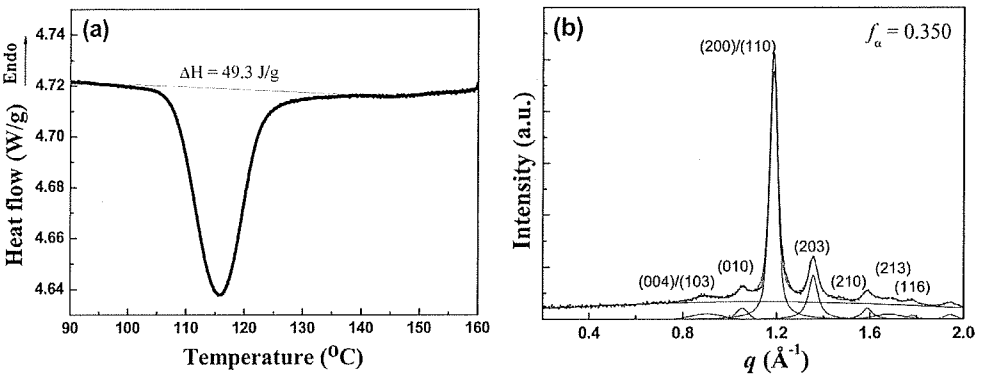

Figure 7. (a) DSC trace for melt-crystallization of PLLA during cooling from 160 to 90 °C at a rate of 1 °C/min. (b) Corresponding WAXS profile obtained by use of an in-house X-ray diffractometer, deconvoluted into a broad amorphous halo and seven reflection peaks of the α crystals. Combination of the two gives an estimate of latent heat $\Delta H_\alpha \approx 49/0.35 \approx 140$ J/g for the ideal, perfectly crystalline α form.

decreases monotonically throughout the cold-crystallization process. Emergence of the 10_7-helix band[23,24] at 922 cm^{-1} around $t_c \approx 200$ s (coinciding with the WAXS-detected incipience of crystallization) and its subsequent development upon weakened absorption in its neighborhood range of 890–940 cm^{-1} are more clearly demonstrated in the magnified view of Figure 6b. The normalized changes in absorbance at 922 and 1267 cm^{-1} are plotted against t_c in Figure 6c, showing generally good correspondence but slightly delayed development of the helical band especially in the very early stage before $t_c \approx 400$ s. It is evident that changes in these two bands are saturated after $t_c \approx 1200$ s, in support of direct α'-to-α transformation during $t_c \approx 1260$–1800 s.

Summary/Comments. To summarize our observations above, the cold-crystallization of glassy PLLA at 80 °C proceeds with decreasing amorphous absorption starting at $t_c \approx 100$ s, followed by emergence of both 10_7 helical band and almost simultaneously the WAXS signals for freshly nucleated α' crystals at $t_c \approx 200$ s. Both the DSC-identified thermal events and SAXS-observed changes emerged only after $t_c \approx 300$ s

dx.doi.org/10.1021/ma501167e | Macromolecules 2014, 47, 5144–5151

(implying low latent heat and density contrast) whereas formation of α crystals of constant lattice constants (signifying its thermodynamic stability) is observed only after $t_c \approx 800$ s. Once formed, α' crystals underwent continuous densification throughout the crystallization process up to $t_c = 2400$ s, with direct α'-to-α transformation clearly identified in the later stage of crystallization (t_c = 1260−1800 s). Note that our observations correspond to the case of isothermal cold-crystallization at a relatively low temperature (ca. 25 °C above the glass transition $T_g \approx 55$ °C); for cold-crystallization upon programmed heating at 5−1800 °C/min, an alternative mechanism of melting−recrystallization of α' crystals into α phase in the temperature range of 150−160 °C has been reported.[25] We note further that the minor presence of α phase at a low crystallization temperature is not limited to the case of cold-crystallization. For example, for PLLA melt-crystallized at $T_c = 90$ °C,[26] the characteristic $(210)_\alpha$ reflection was already present (although weak, indicating the limited content, cf. Figure 6 and 7 therein) before extensive transformation of α' crystals into the α form at 150−165 °C during heating at 2 °C/min.

DISCUSSION

Densification of α' Crystals. The emergence of the strong $(200)/(110)_{\alpha'}$ reflections starts at $t_c \approx 200$ s, approximately 100 s earlier than the first discernible SAXS intensity increase in Figure 1a or the apparent start of crystallization exotherm in Figure 1c, both at $t_c \approx 300$ s. This delayed SAXS response compared to WAXS signals is consistent with SAXS/WAXS profiles reported by Mano et al.[15] (cf. Figures 2 and 4 therein) during cold-crystallization of PLLA upon reheating from the glassy state, although no particular emphasis was given by those authors. The density of glassy PLLA was determined (using the density-gradient column method) as $\rho_{am} = 1.248$ g mL^{-1} at room temperature,[27] while the corresponding value for the crystalline α form can be calculated from the lattice parameters as $\rho_\alpha = 1.280$ g mL^{-1} with a difference of ca. 2.6%. Assuming significant difference in volume expansion of the crystalline and amorphous states mainly above the glass transition ($T_g \approx 55$ °C), one would expect a contrast of ca. 3.4% at 80 °C if the difference in volumetric thermal expansion coefficient is taken as 3×10^{-4} K^{-1}.[28] As deviations in positions of (200)/(110) and (203) reflections of the incipient α' crystals from the corresponding values of the α form are ca. 1.2% and 1.4%, respectively; the expansion in *a*- and *b*-axis are therefore estimated as 1.6% (±0.3%) and 1.1% (±0.5%), respectively, if no change in *c*-axis is assumed. This translates to decreased density of the incipient α' crystals by ca. 2.7% as compared to the α form and a contrast of ca. 0.7% from the melt matrix, one-fifth of that of the α form. Near the end of crystallization, deviations in positions of (200)/(110) and (203) reflections of the better-packed α' crystals from values of the α form are ca. 0.8% and 1.3%, respectively; the expansion in *a*- and *b*-axis are correspondingly decreased to ca. 1.3% (±0.4%) and 0.7% (±0.1%) and hence ca. 2.0% expansion in volume, two-fifth of the contrast of α crystals to the melt matrix. As the SAXS intensity scales with the square of density contrast, these estimated values indicate ca. 1/25 and 4/25 in scattering power (compared to the α form) for incipient and better-packed α' crystals, respectively, in agreement with the initial insensitivity to the freshly emerged α' crystals and the seemingly incessant increases in Q_{SAXS} after saturation of FTIR and WAXS signals.

Latent Heat. The delayed DSC response implies a low value of heat of crystallization ($\Delta H_{\alpha'}$) for incipiently formed α' phase, which is qualitatively consistent with the loose packing of helices. We note first that there are no generally accepted value of the latent heat even for the thermodynamically stable α form. Reported values in the past 4 decades ranged from ca. 80 to 145 J/g,[27,29−33] as the effects from coexisting α' form were often neglected. Given in Figure 7a is the DSC trace for a cooling scan at 1 °C/min from equilibrated melt to 90 °C, during which melt-crystallization of PLLA predominantly into the α form is ensured by the slow cooling process. The corresponding WAXS profile (Figure 7b) obtained at 90 °C then allows for determination of f_α via peak resolution. The combination of these results yields a value of ca. 140 J/g (with a confidence of a few per cents in view of experimental errors in baseline determination etc.) for the idealized α phase of 100% crystallinity. This value is close to the upper end of literature values but significantly higher than the next higher (and more recently reported) value of 106 J/g.[33] For the sake of self-consistency, we adopt our own value in the subsequent discussion; the quantitative difference between 140 and 106 J/g does not affect the qualitative conclusions drawn.

As demonstrated in Figure 5b, there are no α crystals prior to $t_c \approx 720$ s. The total heat released up to this point is found to be 1.41 J/g whereas the corresponding fraction of α' crystallinity is $f_{\alpha'} = 0.115$, leading to $\Delta H_{\alpha'} = 1.41/0.115 \approx 12$ J/g for the freshly emerged α', which is an order-of-magnitude lower than $\Delta H_\alpha \approx 140$ J/g. By the apparent completion of crystallization at $t_c \approx 2400$ s, we have $f_{\alpha'} \approx 0.219$ and $f_\alpha \approx 0.056$, and the total released heat of 24.1 J/g (Figure 1c). These values lead to $\Delta H_{\alpha'} \approx (24.1 - 140 \times 0.056)/0.219 \approx 74$ J/g for α' crystals with improved packing, signifying *major heat release during densification* of α' crystals.

Autoinhibited Conversion. Solid−solid transformation is most dramatically demonstrated by the martensitic transformation between austenite and martensite with good density match such that long-range diffusion is not involved. For crystallization of poly(9,9′-di-*n*-hexylfluorene) during stepwise cooling (at intervals of 15 °C) from equilibrated melt,[34] we have previously shown that the direct transformation from the high-temperature monoclinic phase to the low-temperature triclinic form is limited in conversion due to transformation stresses developed from density mismatch between the two crystalline phases, as demonstrated by extensively transformation-induced cracking. In the present case of density mismatch (ca. 1.4% in the final stage of crystallization at 80 °C) between α' and α forms, transformation-induced stresses are also likely to play a similar role in limiting the conversion of α'-to-α transformation to the composition ratio of f_α:$f_{\alpha'} \approx 1$:4.

Analogy to the Precursory Mesophase. For cold-crystallization of many polymers, a metastable mesomorphic phase (of fairly long life span, significant latent heat, and adequate density contrast with the melt matrix) is often observed to precede the emergence of thermodynamically stable crystals.[8−20] The present case of PLLA cold-crystallization appears to deviate from this general behavior, as the first changes in FTIR and WAXS signals nearly coincide and precede significantly (by more than 100 s) the SAXS-identifiable morphology change due to the low density-contrast of incipient α' crystals. Nevertheless, the clear metastability of the α' phase in terms of its continuous densification and subsequent transformation to stable α crystals bear analogy

dx.doi.org/10.1021/ma501167e | *Macromolecules* 2014, 47, 5144−5151

with the precursory phase in other polymers: both serve as a transient stage to the thermodynamically stable phase.

CONCLUSION

By means of synchrotron-based simultaneous SAXS/WAXS and parallel FTIR/DSC measurements, we investigated the structural/morphological evolution process of PLLA α' crystal during crystallization at 80 °C after a quickly jump (100 °C/min) from the glassy state. We show that α' crystals are intrinsically metastable, release very limited latent heat upon emergence but undergo continuous densification to release a majority of latent heat while partially transform into α crystals, resulting in seemingly incessant increases in the level of global heterogeneity expressed by Q_{SAXS} and apparently delayed heat flow monitored via DSC as compared to morphological changes observed via WAXS and FTIR.

AUTHOR INFORMATION

Corresponding Author

*(A.-C.S.) E-mail: acsu@mx.nthu.edu.tw.

Notes

The authors declare no competing financial interest.

ACKNOWLEDGMENTS

Financial support from the National Science Council (under Grant NSC 101-2221-E-007-037-MY3) is gratefully acknowledged. Thanks are also due to Mr. Wei-Ru Wu in National Synchrotron Radiation Research Center for beamline alignment.

REFERENCES

(1) Wasanasuk, K.; Tashiro, K. *Polymer* **2011**, *52*, 6097–6109 and references cited therein..

(2) Zhang, J.; Duan, Y.; Sato, H.; Tsuji, H.; Noda, I.; Yan, S.; Ozaki, Y. *Macromolecules* **2005**, *38*, 8012–8021.

(3) Di Lorenzo, M. L. *Polymer* **2001**, *42*, 9441–9446.

(4) Di Lorenzo, M. L. *Eur. Polym. J.* **2005**, *41*, 569–575.

(5) Pan, P.; Kai, W.; Zhu, B.; Dong, T.; Inoue, Y. *Macromolecules* **2007**, *40*, 6898–6905.

(6) Cho, T.-Y.; Strobl, G. *Polymer* **2006**, *47*, 1036–1043.

(7) Kawai, T.; Rahman, N.; Matsuba, G.; Nishida, K.; Kanaya, T.; Nakano, M.; Okamoto, H.; Kawada, J.; Usuki, A.; Honma, N. *Macromolecules* **2007**, *40*, 9463–9469.

(8) Schultz, J. M.; Lin, J. S.; Hendricks, R. W.; Petermann, J.; Gohil, R. M. *J. Polym. Sci., Polym. Phys.* **1981**, *19*, 609–620.

(9) Imai, M.; Kaji, K.; Kanaya, T. *Phys. Rev. Lett.* **1993**, *71*, 4162–4165.

(10) Fougnies, C.; Damman, P.; Villers, D.; Dosiere, M.; Koch, M. H. J. *Macromolecules* **1997**, *30*, 1385–1391.

(11) Terrill, N. J.; Fairclough, P. A.; Towns-Andrews, E.; Komanschek, B. U.; Young, R. J.; Ryan, A. J. *Polymer* **1998**, *39*, 2381–2385.

(12) Ryan, A. J.; Fairclough, J. P. A.; Terrill, N. J.; Olmsted, P. D.; Poon, W. C. K. *Faraday Discuss.* **1999**, *112*, 13–29.

(13) Wang, Z.-G.; Hsiao, B. S.; Sirota, E. B.; Srinivas, S. *Polymer* **2000**, *41*, 8825–8832.

(14) Heeley, E. L.; Poh, C. K.; Li, W.; Maidens, A.; Bras, W.; Dolbnya, I. P.; Gleeson, A. J.; Terrill, N. J.; Fairclough, J. P. A.; Olmsted, P. D.; Ristic, R. I.; Hounslow, M. J.; Ryan, A. J. *Faraday Discuss.* **2002**, *122*, 343–361.

(15) Mano, J. F.; Wang, Y.; Viana, J. C.; Denchev, Z.; Oliveira, M. J. *Macromol. Mater. Eng.* **2004**, *289*, 910–915.

(16) Hikosaka, M.; Watanabe, K.; Okada, K.; Yamazaki, S. *Adv. Polym. Sci.* **2005**, *191*, 137–186.

(17) Kaji, K.; Nishida, K.; Kanaya, T.; Matsuba, G.; Konishi, T.; Imai, M. *Adv. Polym. Sci.* **2005**, *191*, 187–240.

(18) Chen, S. H.; Wu, Y. H.; Su, C. H.; Jeng, U.; Hsieh, C. C.; Su, A. C.; Chen, S. A. *Macromolecules* **2007**, *40*, 5353–5359.

(19) Su, C. H.; Jeng, U.; Chen, S. H.; Lin, S. J.; Wu, W. R.; Chuang, W. T.; Tsai, J. C.; Su, A. C. *Macromolecules* **2009**, *42*, 6656–6664.

(20) Chuang, W.-T.; Su, W.-B.; Jeng, U.; Hong, P. D.; Su, C. J.; Su, C. H.; Huang, Y. C.; Laio, K. F.; Su, A. C. *Macromolecules* **2011**, *44*, 1140–1148.

(21) Yang, C. F.; Huang, Y. F.; Ruan, J.; Su, A. C. *Macromolecules* **2012**, *45*, 872–878.

(22) Lund, R.; Alegria, A.; Goitandia, L.; Colmenero, J.; Gonzalez, M. A.; Lindner, P. *Macromolecules* **2008**, *41*, 1364–1376.

(23) Stoclet, G.; Seguela, R.; Lefebvre, J.; Elkoun, S.; Vanmansart, C. *Macromolecules* **2010**, *43*, 1488–1498.

(24) Zhang, J.; Duan, Y.; Domb, A. J.; Ozaki, Y. *Macromolecules* **2010**, *43*, 4240–4246.

(25) Androsch, R.; Schick, C.; Di Lorenzo, M. L. *Macromol. Chem. Phys.* **2014**, *215*, 1134–1139.

(26) Zhang, J.; Tashiro, K.; Tsuji, H.; Domb, A. J. *Macromolecules* **2008**, *41*, 1352–1357.

(27) Fischer, E. W.; Sterzel, H. J.; Wegner, G. *Colloid Polym. Sci.* **1973**, *251*, 980–990.

(28) Van Krevelen *Properties of Polymers*, 3rd ed.; Elsevier: Amsterdam, 1990; Ch. 4.

(29) Gilding, D. K.; Reed, A. M. *Polymer* **1979**, *20*, 1459–1464.

(30) Kalb, B.; Pennings, A. J. *Polymer* **1980**, *21*, 607–612.

(31) Cohn, D.; Younes, H.; Marom, G. *Polymer* **1987**, *28*, 2018–2022.

(32) Loomis, G. L.; Murdoch, J. R.; Gardner, K. H. *Polym. Prepr.* **1990**, *39* (2), 55.

(33) Sarasua, J.-R.; Prud'homme, R. E.; Wisniewski, M.; Le Borgne, A.; Spassky, N. *Macromolecules* **1998**, *31*, 3895–3905.

(34) Chen, S. H.; Su, A. C.; Su, C. H.; Chen, S. A. *J. Phys. Chem. B* **2006**, *110*, 4007–4013.